

Article

First Principles Study on the Effect of Pressure on the Structure, Elasticity, and Magnetic Properties of Cubic GaFe(CN)₆ Prussian Blue Analogue

Chuankun Zhang, Haiming Huang *  and Shijun Luo

School of Science, Hubei University of Automotive Technology, Shiyan 442002, China;
zhangchk_lx@huat.edu.cn (C.Z.); luosjhuat@163.com (S.L.)

* Correspondence: smilehbm@163.com

Received: 17 March 2019; Accepted: 16 April 2019; Published: 18 April 2019



Abstract: The structure, elasticity, and magnetic properties of Prussian blue analogue GaFe(CN)₆ under external pressure ranges from 0 to 40 GPa were studied by first principles calculations. In the range of pressure from 0 to 35 GPa, GaFe(CN)₆ not only has the half-metallic characteristics of 100% spin polarization, but also has stable mechanical properties. The external pressure has no obvious effect on the crystal structure and anisotropy of GaFe(CN)₆, but when the pressure exceeds 35 GPa, the half-metallicity of GaFe(CN)₆ disappears, the mechanical properties are no longer stable, and total magnetic moments per formula unit are no longer integer values.

Keywords: half-metallic material; first principles; Prussian blue analogue; pressure

1. Introduction

Whether spin-polarized electrons can be efficiently injected into semiconductor materials is one of the key technologies to realize spintronic devices [1–6]. Previous studies have shown that magnetic materials with high spin polarizability can effectively inject spin-polarized electrons [7–10]. Half-metallic ferromagnets with a high Curie temperature and nearly 100% spin polarizability undoubtedly become the most ideal spin electron injection source for semiconductors. Among the two different spin channels of half-metallic ferromagnets, one spin channel is metallic, while the other is insulating or a semiconductor [11]. Half-metallic ferromagnets are widely used in spin diodes, spin valves, and spin filters because of their unique electronic structure [12–15].

Since the first half-metallic ferromagnet was predicted by theory, after more than 30 years of development, half-metallic ferromagnetic materials have become a hot topic in materials science and condensed matter physics. Up to now, half-metallic ferromagnets have been found mainly as follows: ternary metal compounds represented by Heulser alloy [16–19], magnetic metal oxides [20,21], perovskite compounds [22,23], dilute magnetic semiconductors [24,25], zinc-blende type pnictides and chalcogenides [26,27], organic–inorganic hybrid compounds [28,29]. Even some two-dimensional materials have half-metallic ferromagnets [30–33].

Prussian blue analogs are a class of metal-organic frameworks with a simple cubic structure, whose chemical formula can be expressed as A₂M[M(CN)₆] (A = alkaline metal ions, zeolitic water; M/M' = Fe, Co, Mn, etc.) [34]. Prussian blue analogs often have simpler molecular configurations due to the existence of vacancy defects. In Prussian blue analogs, there is a large space between metal ions and -CN- groups, which can effectively accommodate alkali metal ions such as Li⁺, Na⁺, and K⁺. The open structure of Prussian blue analogs makes it exhibit excellent electrochemical performance [35–37].

The magnetic study of Prussian blue analogs has also attracted people's attention for a long time. In 1999, Holmes et al. reported a compound KV[Cr(CN)₆] with a Curie temperature as high as

376 K [38]. In 2003, Sato et al. proposed that electrochemical methods could be used to control the magnetism and Curie temperature of Prussian blue analogs [39]. They also pointed out that it was feasible and promising to control the magnetism of Prussian blue analogs by light. Half-metals have also been found in these compounds by studying the magnetism. Two well-defined Prussian blue analogues are predicted as half-metallicity using first principles [40]. In the present study, we will study the structure, elasticity, and magnetic properties of a new Prussian blue analogue $\text{GaFe}(\text{CN})_6$ under pressure and predict that the compound is half-metallic.

2. Materials and Methods

The projector augmented wave (PAW) [41] method encoded in the software Vienna Ab initio Simulation Package (VASP) [42] was performed during the calculations. The generalized gradient approximation (GGA) of the Perdew–Burke–Ernzerhof (PBE) functional is used as exchange correlation potential [43]. The electronic configurations— $4s^2 4p^1$ for Ga, $4s^2 3d^6$ for Fe, $2s^2 2p^2$ for C, and $2s^2 2p^3$ for N—were treated as valence electrons in calculations. For the self-consistent calculation, the plane wave cutoff energy was chosen to be 400 eV. A mesh of $9 \times 9 \times 9$ Monkhorst–Pack k-point was used. The convergence tolerances were selected as the difference in total energy and the maximum force within 1.0×10^{-5} eV and 1.0×10^{-2} eV/atom, respectively.

3. Results and Discussion

Crystal structure characterization based on high resolution synchrotron radiation X-ray diffraction shows that the Prussian blue analogue of $\text{GaFe}(\text{CN})_6$ is a cubic crystal with space group $Fm\bar{3}m$, as shown in Figure 1. The structure of $\text{GaFe}(\text{CN})_6$ is formed with FeC_6 and GaN_6 octahedrons, which are equivalent to ABX_3 type perovskite with vacancy in A site. In the structure of $\text{GaFe}(\text{CN})_6$, the $-\text{Ga}-\text{N}\equiv\text{C}-\text{Fe}-$ chain is formed between gallium, carbon, nitrogen, and iron atoms. Experimentally, the lattice constant of $\text{GaFe}(\text{CN})_6$ was measured as 10.0641 Å at 273 K [36], and the occupied positions of each atom in the structure are shown in Table 1.

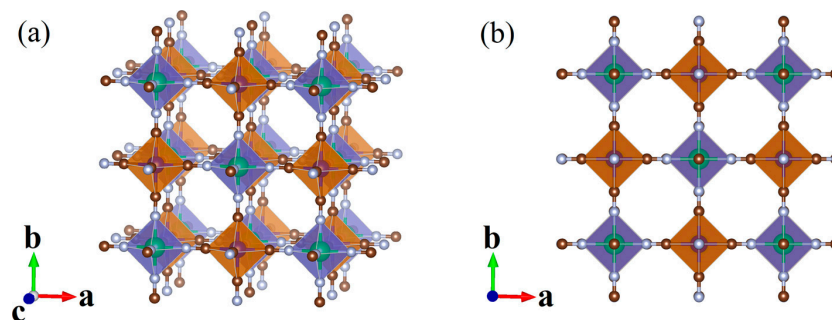


Figure 1. Crystal structure of $\text{GaFe}(\text{CN})_6$. (a) Side view; (b) top view.

Table 1. Atomic occupied positions in $\text{GaFe}(\text{CN})_6$.

Atom	Exp.			Present		
	x	y	z	x	y	z
Ga	0.0	0.0	0.0	0.0	0.0	0.0
Fe	0.5	0.0	0.0	0.5	0.0	0.0
C	0.3043	0.0	0.0	0.3253	0.0	0.0
N	0.1883	0.0	0.0	0.2114	0.0	0.0

In order to obtain the theoretical equilibrium lattice constant and the ground state properties of $\text{GaFe}(\text{CN})_6$, we constructed supercells based on experimental structural parameters and calculated the total energy of ferromagnetic (FM), non-magnetic (NM), and antiferromagnetic (AFM) states of $\text{GaFe}(\text{CN})_6$ under different lattice constants. The ground state is determined based on the principle

that the lower the energy is, the more stable the structure is. The total energies of GaFe(CN)₆ in FM, NM, and AFM states are drawn in Figure 2. Obviously, FM states have lower total energy than NM and AFM states, which means the ferromagnetic state is the most stable for GaFe(CN)₆. The equilibrium lattice constant obtained at the same time was 10.1883 Å. This result is slightly larger than the experimental result, and the deviation is 1.23% compared with the experimental result, which is within a reasonable range. The coordinates of the positions of the atoms in the equilibrium state of GaFe(CN)₆ are also listed in Table 1. Excepting that the x coordinates of C and N atoms deviate from the experimental data, the other results are consistent with the experimental values.

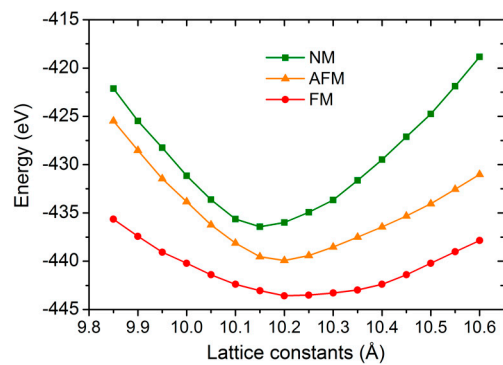


Figure 2. The total energies of GaFe(CN)₆ in ferromagnetic (FM), non-magnetic (NM), and antiferromagnetic (AFM) states.

In order to study the effect of pressure on the crystal structure of GaFe(CN)₆, the pressure measurement of GaFe(CN)₆ was carried out at intervals of 5.0 GPa under pressure of 0–40 GPa. The variation of relative lattice constant a/a_0 and relative volume V/V_0 with pressure was obtained, as shown in Figure 3. Among them, a_0 is the equilibrium lattice constant at 0 GPa and V_0 is the cell volume at 0 GPa. As can be seen from Figure 3, the lattice constant decreases gradually with the increase of external pressure, resulting in the corresponding decrease of volume V and relative volume V/V_0 .

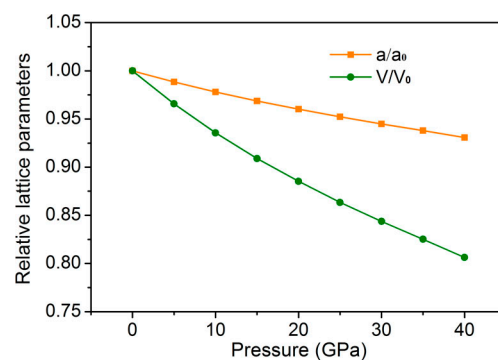


Figure 3. The variation of relative lattice constant a/a_0 and relative volume V/V_0 with pressure.

In order to further understand the variation of structural parameters with pressure, the curve of Figure 3 is fitted and calculated, and the binary quadratic state equations of a/a_0 and V/V_0 of GaFe(CN)₆ and pressure are obtained, as shown below.

$$a/a_0 = 0.99645 - 0.00171P + 5.71387 \times 10^{-5}P^2 \quad (1)$$

$$V/V_0 = 0.98777 - 0.00475P + 4.05769 \times 10^{-4}P^2 \quad (2)$$

Table 2 gives the structural parameters of GaFe(CN)₆ under pressure. The lattice constant at 40 GPa is 9.4828 Å, which is only 93.1% of the lattice constant at 0 GPa. The bond lengths of C–N,

Ga–N, and Fe–C in the compounds decrease with the increase of pressure, which is mainly due to the compression of the volume of the compounds under pressure and the reduction of the spacing between atoms. The pressure from 0 to 40 GPa does not cause structural transition of GaFe(CN)₆, because GaFe(CN)₆ still presents a cubic phase structure. Except for the x-direction coordinates of C and N atoms, the positions or coordinates of other atoms in compounds have not changed.

Table 2. Structural parameters of GaFe(CN)₆ under different pressures.

Pressure	a (Å)	C–N(Å)	Ga–N(Å)	Fe–C(Å)	C(x,0,0)	N(x,0,0)
0	10.1883	1.160	2.155	1.780	0.32533	0.21148
5	10.0706	1.156	2.118	1.762	0.32508	0.21029
10	9.9649	1.152	2.085	1.745	0.32492	0.20928
15	9.8695	1.149	2.057	1.729	0.32481	0.20843
20	9.7830	1.145	2.028	1.719	0.32430	0.20728
25	9.7015	1.142	2.008	1.701	0.32471	0.20701
30	9.6271	1.138	1.987	1.688	0.32461	0.20636
35	9.5563	1.135	1.967	1.676	0.32459	0.20579
40	9.4828	1.132	1.945	1.665	0.32447	0.20512

The elastic constants are important parameters reflecting the mechanical stability of the compounds [44,45]. At 0 GPa, the elastic constants C_{11} , C_{12} , and C_{44} of GaFe(CN)₆ are 206.7, 53.2, and 54.6 GPa, respectively. The mechanical stability Born–Huang criteria of cubic crystal are expressed as [46,47]:

$$C_{11} - C_{12} > 0, C_{11} + 2C_{12} > 0, C_{44} > 0. \quad (3)$$

The elastic constants of GaFe(CN)₆ at 0 GPa satisfy the above conditions, which means that GaFe(CN)₆ has stable mechanical properties in an equilibrium state. At the same time, it was noted that the unidirectional elastic constant C_{11} is higher than C_{44} , which indicates that GaFe(CN)₆ has weaker resistance to the pure shear deformation compared to the resistance of the unidirectional compression.

Some mechanical parameters can be calculated by elastic constants according to some formulas, which can be obtained in our previous studies [48]. The elastic anisotropy factor A is calculated by the following formula:

$$A = 2C_{44}/(C_{11} - C_{12}). \quad (4)$$

The elastic anisotropy factor A of GaFe(CN)₆ is 0.71; it is usually used to quantify the elastic anisotropy and the degree of elastic anisotropy of the compound. In general, the elastic anisotropic factor for isotropic crystals is $A = 1$, while for anisotropic crystals $A \neq 1$. According to this criterion, GaFe(CN)₆ is an anisotropic compound. The Poisson's ratio, which reflects the binding force characteristics, is often between 0.25 and 0.50. The Poisson's ratio of GaFe(CN)₆ is 0.25, which is just in the range of values, meaning that the inter-atomic forces are central for the compounds. The Debye temperature of the GaFe(CN)₆ is 738.4 K, which is calculated from a formula in [47,49].

Under the isotropic pressure, the elastic constants are transformed into the corresponding stress–strain coefficients by the following expressions:

$$B_{11} = C_{11} - P, B_{12} = C_{12} + P, B_{44} = C_{44} - P. \quad (5)$$

The mechanical stability of GaFe(CN)₆ under isotropic pressure is determined by the following formula [48,50]:

$$B_{11} - B_{12} > 0, B_{11} + 2B_{12} > 0, B_{44} > 0. \quad (6)$$

The P in the formula above refers to the external pressure. The curves of $B_{11} - B_{12}$, $B_{11} + 2B_{12}$, and B_{44} with pressure are plotted in Figure 4. $B_{11} - B_{12}$ and $B_{11} + 2B_{12}$ increase with the increase of pressure, and also meet the mechanical stability criterion under pressure. When the pressure is greater than 35 GPa, the value of B_{44} is negative, and the stability condition of B_{44} is not satisfied. Generally

speaking, when the external pressure of $\text{GaFe}(\text{CN})_6$ is less than 35 GPa, its mechanical performance is stable. Once the external pressure exceeds 35 GPa, the mechanical performance of $\text{GaFe}(\text{CN})_6$ is unstable.

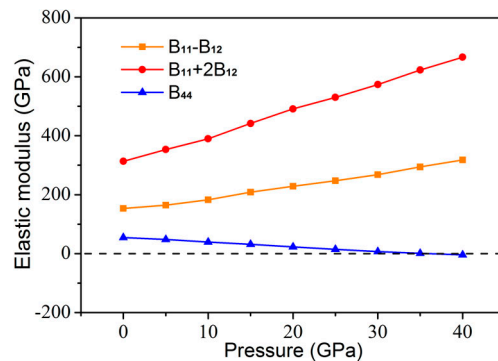


Figure 4. Elastic modulus of $\text{GaFe}(\text{CN})_6$ under different pressures.

From 0 to 40 GPa, elastic anisotropy factor A becomes smaller and smaller, and the anisotropic characteristics of $\text{GaFe}(\text{CN})_6$ become more obvious. At the same time, the bulk modulus increases from 104.3 to 208.8 GPa, and the Debye temperature reaches 798.5 K. The increase in pressure makes the atoms more closely linked, which makes the compound's stiffness.

The spin-polarized band structures and density of states of $\text{GaFe}(\text{CN})_6$ at 0 GPa are depicted in Figure 5. It can be clearly seen that the conduction band minimum (CBM) and valence band maximum (VBM) in majority-spin are located at the same highly symmetric G-point, and a band gap of 4.01 eV is formed between the conduction band and the valence band, indicating that this spin direction has insulator behavior. The bands pass through the Fermi level in minority-spin to exhibit a metallic feature. According to the band theory of quantum solid, $\text{GaFe}(\text{CN})_6$ is a half-metal with 100% spin polarization.

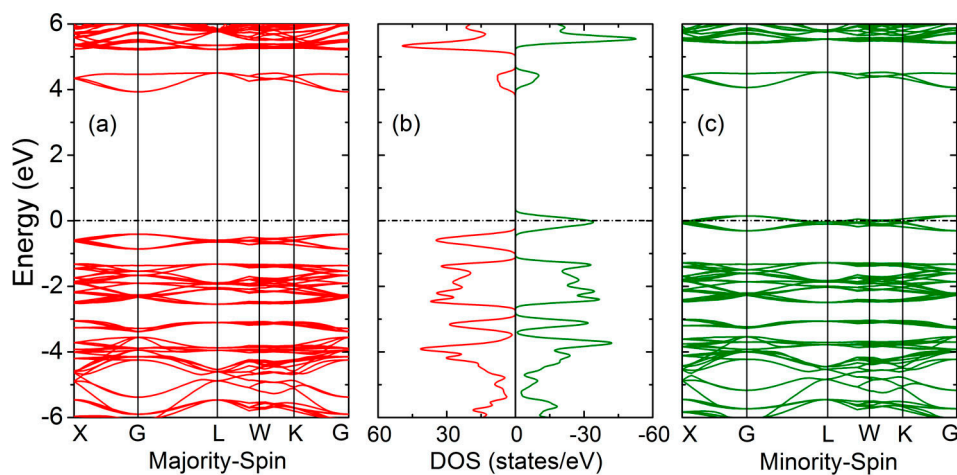


Figure 5. Band structure and density of states (DOS) of $\text{GaFe}(\text{CN})_6$ at 0 GPa.

Figure 6 presents the total and local density of state of $\text{GaFe}(\text{CN})_6$ at 0 GPa. It can be clearly seen that the half-metallic behavior of $\text{GaFe}(\text{CN})_6$ is mainly due to the formation of spin splitting in the vicinity of the Fermi level by the 3d states of the Fe atom and the 2p states of the N atom. The 3d states of the Fe atom and the 2p states of the N atom have obvious spin hybridization in the energy range of -1.01 to 0.35 eV. The 3d state of the Fe atom is also the most important contributor to the total density of $\text{GaFe}(\text{CN})_6$. From the magnetic properties generated by spin splitting, it can be inferred that Fe atoms are also the main source of $\text{GaFe}(\text{CN})_6$ magnetic moment. In the energy range of -2.7 to -1.01 eV, the density of states is mainly derived from the C-2p, N-2p, and Ga-4p states, and the 3d of the Fe atom has little contribution in this region.

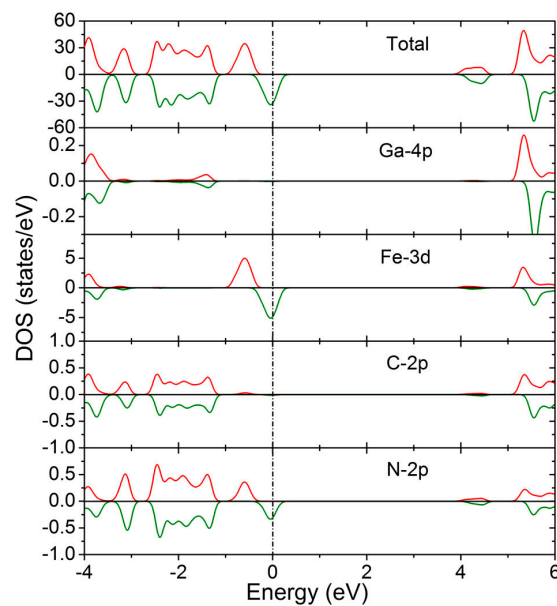


Figure 6. Total and local density of states of $\text{GaFe}(\text{CN})_6$ at 0 GPa.

The electronic structure calculation of pressure from 0 to 40 GPa shows that the minority-spin direction of $\text{GaFe}(\text{CN})_6$ always shows metallic behavior. In this case, the physical properties of $\text{GaFe}(\text{CN})_6$ under pressure are basically determined by the majority-spin electronic states. Figure 7 depicts the CBM and VBM in majority-spin of $\text{GaFe}(\text{CN})_6$ as a function of pressure. With the increase of pressure, both CBM and VBM move towards high energy. Once the pressure is greater than 35 GPa, VBM will cross the Fermi level and make $\text{GaFe}(\text{CN})_6$ majority-spin also show metallic behavior. In this way, the half-metallicity of $\text{GaFe}(\text{CN})_6$ will disappear. It is worth noting that, as can be seen from Figure 7, the density of states across the Fermi level at 40 GPa is very low. This means that the material may not be able to hold enough free electrons and therefore has poor conductivity or metallicity.

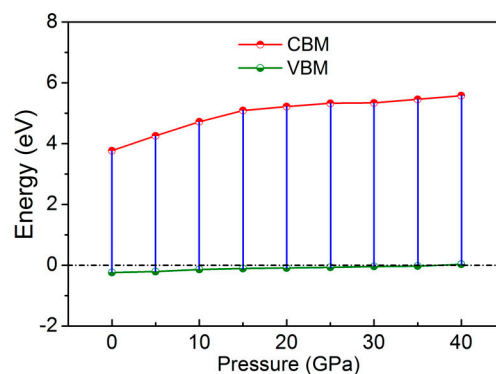


Figure 7. Conduction band minimum (CBM) and valence band maximum (VBM) of $\text{GaFe}(\text{CN})_6$ in majority-spin under different pressures.

The effect of pressure on the electronic structure of $\text{GaFe}(\text{CN})_6$ can also be confirmed by Figure 8. In Figure 8, we can see that the minority-spin electronic states are hardly affected by external pressures. A slightly more obvious feature is that the conduction band in the high energy region moves toward a higher energy position as the pressure increases. However, this does not change the metallicity of the minority-spin direction. The electronic structure in majority-spin changes are consistent with the analysis in Figure 7. When the pressure is 40 GPa, the valence band in majority-spin crosses the Fermi level.

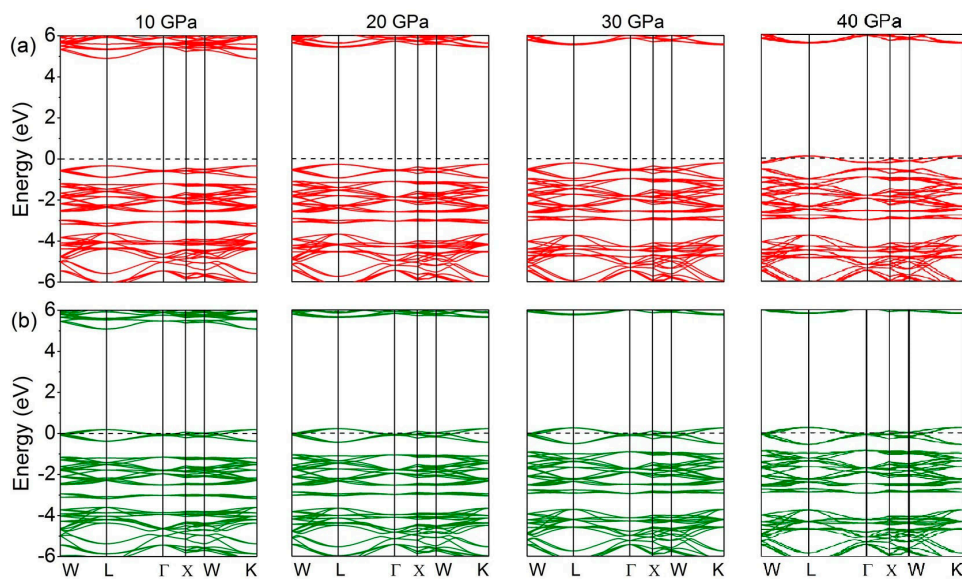


Figure 8. Band structure of GaFe(CN)₆ under different pressures. (a) Majority-spin; (b) minority-spin.

At 0 GPa, the total magnetic moment per formula unit of GaFe(CN)₆ is 1.0 μ_B , which is very consistent with the characteristic that the molecular magnetic moment of half-metallic magnetic materials is an integral value. The local magnetic moments of Fe, Ga, C, and N atoms are 0.765 μ_B , $-0.007 \mu_B$, $-0.018 \mu_B$, and 0.035 μ_B , respectively. Obviously, Fe atoms are the most important contributors to the magnetic properties of GaFe(CN)₆. The local magnetic moments of Ga, C, and N atoms are very small. Because these three atoms have no magnetism, their magnetic moments are mainly induced by the influence of the Fe atom. In $-\text{Ga}-\text{N}-\text{C}-\text{Fe}-$ chemical chains, the local magnetic moments between them show a sign change of $-/+/-/+$, which means that there is antiferromagnetic coupling between these atoms.

Figure 9 shows the total and local magnetic moments of GaFe(CN)₆ under pressure. From 0 to 35 GPa, the total magnetic moment per formula unit of GaFe(CN)₆ is 1.0 μ_B . In this pressure range, GaFe(CN)₆ has half-metal characteristics. When the pressure exceeds 35 GPa, GaFe(CN)₆ is no longer a half-metal and its molecular magnetic moment is no longer an integral value. The local magnetic moment of the Fe atom decreases with the increase of pressure, while the induced magnetic moment of the N atom increases slightly, although its value is very small. The local magnetic moments of Ga and C atoms are hardly affected by pressure. From the local magnetic moment signs of Ga, N, C, and Fe atoms, the change of pressure has no effect on the antiferromagnetic coupling of $-\text{Ga}-\text{N}-\text{C}-\text{Fe}-$ chemical chains.

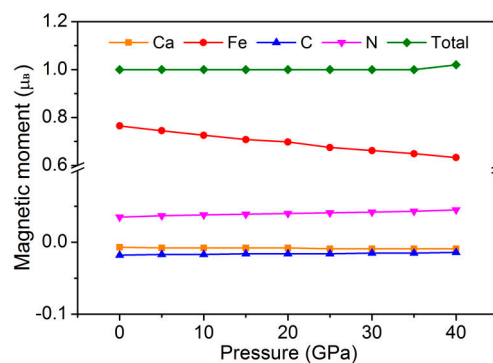


Figure 9. Total and local magnetic moments of GaFe(CN)₆ under pressure.

4. Conclusions

First principles calculations were performed to study the structure, elasticity, and magnetism of a Prussian blue analogue $\text{GaFe}(\text{CN})_6$ under external pressure ranges from 0 to 40 GPa. The crystal structure obtained by theoretical optimization was very close to the experimental structure, and the external pressure had no obvious effect on the cubic structure of $\text{GaFe}(\text{CN})_6$. In the range of pressure from 0 to 35 GPa, $\text{GaFe}(\text{CN})_6$ was an anisotropic compound with stable mechanical properties. It also was a half-metallic magnetic material with 100% spin polarization, and its total magnetic moment per formula unit was $1.0 \mu_B$. When the pressure exceeded 35 GPa, the mechanical properties were no longer stable, the half-metallicity of $\text{GaFe}(\text{CN})_6$ disappeared, and the magnetic moment no longer had the typical characteristics of half-metallic magnetic materials, that is, the total magnetic moment per formula unit was no longer an integer value. In terms of magnetism, iron atoms are the most important contributors to $\text{GaFe}(\text{CN})_6$ magnetism in the whole pressure range.

Author Contributions: Methodology, C.Z.; investigation, H.H.; writing-original draft preparation, H.H.; writing-review and editing, C.Z.; project administration, S.J.

Funding: This work is supported by the Natural Science Foundation of Hubei Province (No. 2017CFB740), the Doctoral Scientific Research Foundation of Hubei University of Automotive Technology (No. BK201804), the Scientific Research Items Foundation of Hubei Educational Committee (No. Q20111801).

Conflicts of Interest: The authors declare no conflict of interest.

References

1. Wolf, S.A.; Awschalom, D.D.; Buhrman, R.A.; Daughton, J.M.; von Molnár, S.; Roukes, M.L.; Chtchelkanova, A.Y.; Treger, D.M. Spintronics: A spin-based electronics vision for the future. *Science* **2001**, *294*, 1488–1495. [[CrossRef](#)] [[PubMed](#)]
2. Kioseoglou, G.; Hanbicki, A.T.; Sullivan, J.M.; Erve, O.M.J.; Li, C.H.; Erwin, S.C.; Mallory, R.; Yasar, M.; Petrou, A.; Jonker, B.T. Electrical spin injection from an n-type ferromagnetic semiconductor into a III–V device heterostructure. *Nat. Mater.* **2004**, *3*, 799–803. [[CrossRef](#)] [[PubMed](#)]
3. Jonker, B.T. Progress toward electrical injection of spin-polarized electrons into semiconductors. *IEEE Proc.* **2003**, *91*, 727–740. [[CrossRef](#)]
4. Zutic, I.; Fabian, J.; Das Sarma, S. Spintronics: Fundamentals and applications. *Rev. Mod. Phys.* **2004**, *76*, 323–410. [[CrossRef](#)]
5. Prinz, G.A. Magnetoelectronics. *Science* **1998**, *282*, 1660–1663. [[CrossRef](#)] [[PubMed](#)]
6. Flatte, M.E.; Beyers, J.M. Spin diffusion in semiconductors. *Phys. Rev. Lett.* **2000**, *84*, 4220–4223. [[CrossRef](#)]
7. Farshchi, R.; Ramsteiner, M. Spin injection from Heusler alloys into semiconductors: A materials perspective. *J. Appl. Phys.* **2013**, *113*, 191101. [[CrossRef](#)]
8. Medvedeva, J.E.; Freeman, A.J.; Cui, X.Y.; Stampfl, C.; Newman, N. Half-Metallicity and Efficient Spin Injection in AlN/GaN:Cr (0001) Heterostructure. *Phys. Rev. Lett.* **2005**, *94*, 146602. [[CrossRef](#)]
9. De Wijs, G.A.; De Groot, R.A. Towards 100% spin-polarized charge-injection: The half-metallic NiMnSb/CdS interface. *Phys. Rev. B* **2001**, *64*, 020402. [[CrossRef](#)]
10. Li, J.; Gao, G.Y.; Min, Y.; Yao, K.L. Half-metallic YN_2 monolayer: Dual spin filtering, dual spin diode and spin seebeck effects. *Phys. Chem. Chem. Phys.* **2016**, *18*, 28018–28023. [[CrossRef](#)]
11. De Groot, R.A.; Mueller, F.M.; Van Engen, P.G.; Buschow, K.H.J. New Class of Materials: Half-Metallic Ferromagnets. *Phys. Rev. Lett.* **1983**, *50*, 2024. [[CrossRef](#)]
12. Han, J.; Shen, J.; Gao, G. CrO_2 -based heterostructure and magnetic tunnel junction: Perfect spin filtering effect, spin diode effect and high tunnel magnetoresistance. *RSC Adv.* **2019**, *9*, 3550–3557. [[CrossRef](#)]
13. Song, Y.; Dai, G. Spin filter and spin valve in ferromagnetic graphene. *Appl. Phys. Lett.* **2015**, *106*, 223104. [[CrossRef](#)]
14. Everschor-Sitte, K.; Sitte, M.; MacDonald, A.H. Half-metallic magnetism and the search for better spin valves. *J. Appl. Phys.* **2014**, *116*, 083906. [[CrossRef](#)]
15. Stefano, S. Molecular spintronics. *Chem. Soc. Rev.* **2011**, *40*, 3336–3355.

16. Chen, Y.; Chen, S.; Wang, B.; Wu, B.; Huang, H.; Qin, X.; Li, D.; Yan, W. Half-Metallicity and Magnetism of the Quaternary Heusler Compound $\text{TiZrCoIn}_{1-x}\text{Ge}_x$ from the First-Principles Calculations. *Appl. Sci.* **2019**, *9*, 620. [[CrossRef](#)]
17. Huang, H.M.; Luo, S.J.; Yao, K.L. Half-metallicity and tetragonal distortion in semi-heusler alloy FeCrSe . *J. Appl. Phys.* **2014**, *115*, 043713. [[CrossRef](#)]
18. Wang, X.T.; Dai, X.F.; Wang, L.Y.; Liu, X.F.; Wang, W.H.; Wu, G.H.; Tang, C.C.; Liu, G.D. Electronic structures and magnetism of Rh_3Z ($\text{Z}=\text{Al, Ga, In, Si, Ge, Sn, Pb, Sb}$) with DO_3 structures. *J. Magn. Magn. Mater.* **2015**, *378*, 16–23. [[CrossRef](#)]
19. Feng, L.; Ma, J.; Yang, Y.; Lin, T.; Wang, L. The electronic, magnetic, half-metallic and mechanical properties of the equiatomic quaternary heusler compounds FeRhCrSi and FePdCrSi : A first-Principles Study. *Appl. Sci.* **2018**, *8*, 2370. [[CrossRef](#)]
20. Schwarz, K. CrO_2 predicted as a half-metallic ferromagnet. *J. Phys. F Met. Phys.* **1986**, *16*, L211–L215. [[CrossRef](#)]
21. Kim, W.; Kawaguchi, K.; Koshizaki, N. Fabrication and magnetoresistance of tunnel junctions using half-metallic Fe_3O_4 . *J. Appl. Phys.* **2003**, *93*, 8032–8034. [[CrossRef](#)]
22. Huang, H.M.; Jiang, Z.Y.; Lin, Y.M.; Zhou, B.; Zhang, C.K. Design of half-metal and spin gapless semiconductor for spintronics application via cation substitution in methylammonium lead iodide. *Appl. Phys. Express* **2017**, *10*, 123002. [[CrossRef](#)]
23. Lv, S.H.; Li, H.P.; Liu, X.J.; Han, D.M.; Wu, Z.J.; Meng, J.A. new half-metallic ferromagnet $\text{La}_2\text{NiFeO}_6$: Predicted from first-principles calculations. *J. Phys. Chem. C* **2010**, *114*, 16710–16715. [[CrossRef](#)]
24. Haneef, M.; Arif, S.; Akbar, J.; Abdul-Malik, A. Theoretical investigations of half-metallicity in Cr-substituted $\text{GaN, GaP, GaAs, GaSb}$ material systems. *J. Electron. Mater.* **2014**, *43*, 3169–3176. [[CrossRef](#)]
25. Liu, H.; Zhang, J.M. Effect of two identical 3d transition-metal atoms M doping ($\text{M}=\text{V, Cr, Mn, Fe, Co, and Ni}$) on the structural, electronic, and magnetic properties of ZnO . *Phys. Status Solidi B* **2017**, *254*, 1700098. [[CrossRef](#)]
26. Gao, G.Y.; Yao, K.L.; Sasioglu, E.; Sandratskii, L.M.; Liu, Z.L.; Jiang, J.L. Half-metallic ferromagnetism in zinc-blende CaC, SrC, and BaC from first principles. *Phys. Rev. B* **2007**, *75*, 174442. [[CrossRef](#)]
27. Xie, W.H.; Xu, Y.Q.; Liu, B.G.; Pettifor, D.G. Half-metallic ferromagnetism and structural stability of zincblende phases of the transition-metal chalcogenides. *Phys. Rev. Lett.* **2003**, *91*, 037204. [[CrossRef](#)]
28. Yao, K.L.; Zhu, L.; Liu, Z.L. First-principles study of the ferromagnetic and half metallic properties of the fumarate-bridged polymer. *Eur. Phys. J. B* **2004**, *39*, 283–286. [[CrossRef](#)]
29. Huang, H.M.; Luo, S.J.; Liu, G.Y.; Yao, K.L. First-principles study of electronic structure and half-metallicity of molecule-based ferromagnet $\text{Cr}[\text{N}(\text{CN})_2]_2$. *Chin. J. Chem. Phys.* **2011**, *24*, 189–193. [[CrossRef](#)]
30. Zheng, J.M.; He, R.J.; Wan, Y.; Zhao, P.J.; Guo, P.; Jiang, Z.Y. Half-metal state of a Ti_2C monolayer by asymmetric surface decoration. *Phys. Chem. Chem. Phys.* **2019**, *21*, 3318–3326. [[CrossRef](#)] [[PubMed](#)]
31. Wang, Y.P.; Li, S.S.; Zhang, C.W.; Zhang, S.F.; Ji, W.X.; Li, P.; Wang, P.J. High-temperature Dirac half-metal PdCl_3 : A promising candidate for realizing quantum anomalous Hall effect. *J. Mater. Chem. C* **2018**, *6*, 10284–10291. [[CrossRef](#)]
32. Lv, P.; Tang, G.; Yang, C.; Deng, J.M.; Liu, Y.Y.; Wang, X.Y.; Wang, X.Q.; Hong, J.W. Half-metallicity in two-dimensional Co_2Se_3 monolayer with superior mechanical flexibility. *2D Mater.* **2018**, *5*, 045026. [[CrossRef](#)]
33. Gao, Q.; Wang, H.L.; Zhang, L.F.; Hu, S.L.; Hu, Z.P. Computational study on the half-metallicity in transition metal-oxide-incorporated 2D $\text{g-C}_3\text{N}_4$ nanosheets. *Front. Phys.* **2018**, *13*, 138108. [[CrossRef](#)]
34. Deng, L.; Yang, Z.; Tan, L.; Zeng, L.; Zhu, Y.; Guo, L. Investigation of the Prussian Blue Analog $\text{Co}_3[\text{Co}(\text{CN})_6]_2$ as an Anode Material for Nonaqueous Potassium-Ion Batteries. *Adv. Mater.* **2018**, *30*, 1802510. [[CrossRef](#)] [[PubMed](#)]
35. Sun, D.; Wang, H.; Deng, B.; Zhang, H.; Wang, L.; Wan, Q.; Yan, X.; Qu, M. A Mn Fe based Prussian blue Analogue@Reduced graphene oxide composite as high capacity and superior rate capability anode for lithium-ion batteries. *Carbon* **2019**, *143*, 706–713. [[CrossRef](#)]
36. Gao, Q.; Shi, N.; Sanson, A.; Sun, Y.; Milazzo, R.; Olivi, L.; Zhu, H.; Lapidus, S.H.; Zheng, L.; Chen, J.; Xing, X. Tunable Thermal Expansion from Negative, Zero, to Positive in Cubic Prussian Blue Analogues of $\text{GaFe}(\text{CN})_6$. *Inorg. Chem.* **2018**, *57*, 14027–14030. [[CrossRef](#)] [[PubMed](#)]

37. Xiong, P.; Zeng, G.; Zeng, L.; Wei, M. Prussian blue analogues $\text{Mn}[\text{Fe}(\text{CN})_6]_{0.6667} \cdot n\text{H}_2\text{O}$ cubes as an anode material for lithium-ion batteries. *Dalton Trans.* **2015**, *44*, 16746–16751. [[CrossRef](#)] [[PubMed](#)]
38. Holmes, S.H.; Girolami, G.S. Sol-Gel Synthesis of $\text{KV}^{\text{II}}[\text{Cr}^{\text{III}}(\text{CN})_6] \cdot 2\text{H}_2\text{O}$: A Crystalline Molecule-Based Magnet with a Magnetic Ordering Temperature above 100 °C. *J. Am. Chem. Soc.* **1999**, *121*, 5593–5594. [[CrossRef](#)]
39. Sato, O.; Hayami, S.; Einaga, Y.; Gu, Z.Z. Control of the Magnetic and Optical Properties in Molecular Compounds by Electrochemical, Photochemical and Chemical Methods. *Bull. Chem. Soc. Jpn.* **2003**, *76*, 443–470. [[CrossRef](#)]
40. Wojdel, J.C.; Moreira, I.P.R.; Bromleyac, S.T.; Illas, F. Prediction of half-metallic conductivity in Prussian Blue derivatives. *J. Mater. Chem.* **2009**, *19*, 2032–2036. [[CrossRef](#)]
41. Blöchl, P.E. Projector augmented-wave method. *Phys. Rev. B* **1994**, *50*, 17953. [[CrossRef](#)]
42. Kresse, G.; Furthmüller, J. Efficiency of ab-initio total energy calculations for metals and semiconductors using a plane-wave basis set. *Comput. Mater. Sci.* **1996**, *6*, 15–50. [[CrossRef](#)]
43. Perdew, J.P.; Burke, K.; Ernzerhof, M. Generalized gradient approximation made simple. *Phys. Rev. Lett.* **1996**, *77*, 3865. [[CrossRef](#)] [[PubMed](#)]
44. Zhang, X.D.; Lv, Y.; Liu, C.; Wang, F.; Jiang, W. Site preference of transition-metal elements additions on mechanical and electronic properties of B_2DyCu -based alloys. *Mater. Des.* **2017**, *133*, 476–486. [[CrossRef](#)]
45. Zhang, X.D.; Huang, W.Y.; Ma, H.; Yu, H.; Jiang, W. First-principles prediction of the physical properties of $\text{ThM}_2\text{Al}_{20}$ (M = Ti, V, Cr) intermetallics. *Solid State Commun.* **2018**, *284–286*, 75–83. [[CrossRef](#)]
46. Mehmood, N.; Ahmad, R.; Murtaza, G. Ab initio investigations of structural, elastic, mechanical, electronic, magnetic, and optical properties of half-Heusler compounds RhCrZ (Z = Si, Ge). *J. Supercond. Novel Magn.* **2017**, *30*, 2481–2488. [[CrossRef](#)]
47. Huang, Y.C.; Guo, X.F.; Ma, Y.L.; Shao, H.B.; Xiao, Z.B. Stabilities, electronic and elastic properties of $\text{L1}_2\text{-Al}_3(\text{Sc}_{1-x}\text{Zr}_x)$ with different Zr content: A first-principles study. *Physica B* **2018**, *548*, 27–33. [[CrossRef](#)]
48. Huang, H.M.; Luo, S.J.; Xiong, Y.C. Pressure-induced electronic, magnetic, half-metallic, and mechanical properties of half-Heusler compound CoCrBi . *J. Magn. Magn. Mater.* **2017**, *438*, 5–11. [[CrossRef](#)]
49. Anderson, O.L. A simplified method for calculating the debye temperature from elastic constants. *J. Phys. Chem. Solids* **1963**, *24*, 909–917. [[CrossRef](#)]
50. Allali, D.; Bouhemadou, A.; Zerarga, F.; Ghebouli, M.A.; Bin-Omran, S. Prediction study of the elastic and thermodynamic properties of the SnMg_2O_4 , SnZn_2O_4 and SnCd_2O_4 spinel oxides. *Comput. Mater. Sci.* **2012**, *60*, 217–223. [[CrossRef](#)]

